

# Concept Study of PM Synchronous Motor Drive System in Cow Brush Application

S. Borup, M. Brandt, F. Clausen, A. Langbak, A. Torp

Department of Materials and Production, Aalborg University

Fibigerstraede 16, DK-9220 Aalborg East, Denmark

Email: [skremp14,mibr13,fclaus14,alangb14,atorp14}@student.aau.dk](mailto:skremp14@mibr13.fclaus14.alangb14.atorp14@student.aau.dk),

web page: <http://www.mechman.m-tech.aau.dk/>

---

## Abstract

In this paper a permanent magnet synchronous motor (PMSM) drive system is implemented in a cow brush to investigate the potential of the PMSM as a means of reducing the energy consumption of the device. An experimental setup is constructed by implementing PMSM drive system in a commercial cow brush and for this setup a control system, based on the field oriented control approach, is designed and implemented digitally. Upon successful implementation the PMSM drive system is benchmarked against a line driven single phase induction motor (IM) system typically used for commercial cow brush applications. The PMSM system is found to have a no-load power consumption of just 9 [W] compared to the IM systems 300 [W]. Furthermore the PMSM system is found to have an efficiency of minimum 73 [%] compared to the IM systems 21 [%], at a prescribed realistic load level for the device. The paper concludes that the PMSM does provide significant energy reductions of the device, however further issues must be addressed before transitioning to a PMSM based solution for the cow brush application.

**Keywords:** Motor Drives, PM Synchronous Motor, Field Oriented Control, Inverter, Efficiency

---

## 1 Introduction

Permanent Magnet Synchronous Motor (PMSM) drives are not a new technology, yet due to the high initial costs of these motor drives, they were previously reserved for high performance applications. However, as the costs associated with permanent magnets (PM) are decreasing, the PMSM becomes progressively more competitive with the induction motor (IM) [1]. Consequently, the industrial trend is changing and PMSM drives are becoming a popular choice among design engineers, as they typically offer high torque density, more compact designs and quieter operation, as compared to IM drives [2]. Additionally, the PMs eliminate rotor induction losses, why the efficiency is generally much higher than what can be achieved with a similarly rated IM drive. This property of the PMSM drive is of particular interest in most industrial applications due to ongoing pressure of keeping energy consumption at a minimum.

One application that could potentially benefit from increased efficiency is the automatically rotating cow brush. The popularity of this device is on the

rise, as studies have shown that providing dairy cows with such cow brushes is associated with reduction in diseases, improved animal welfare and increased milk production, among other benefits [3]. Currently, cow brushes are typically driven by IM drives, favored due to the low initial costs and robustness. However, it is estimated that the cow brush operates an average of 12 hours per day [4], why any energy reduction is of considerable relevance and will yield significant monetary gains during the product lifespan.

This paper thus seeks to investigate the potential of introducing a PMSM drive in a cow brush, as a means of reducing its energy consumption.

## 2 Cow Brush Transmission System

The specific PM synchronous motor selected for the application is a high-torque, low-speed 230 [V] motor of type 120TYDS214. With a rated torque of 5.5 [Nm] and a rated speed of 215 [rpm], it is conveniently combined with a 6:1 geared belt drive to yield the desired brush speed of approximately 35 [rpm] and torque of 33 [Nm], when operated at rated

conditions. Figure 1 shows the cow brush and the physical layout of the PMSM drive implemented in the cow brush. The mechanical setup is considered beyond the scope of this paper, why the physical implementation of the transmission system is only considered a proof of concept and has thus not been subjected to extensive design considerations or dimensioning.

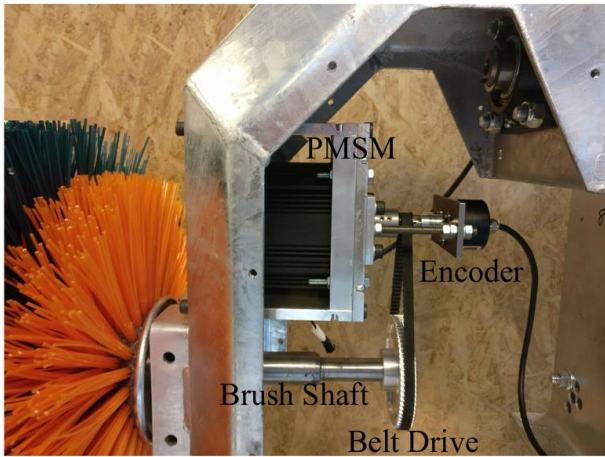


**Fig.1.** Physical layout of the transmission system in the cow brush.

The selected PMSM is a 3-phase star connected motor with a physical layout similar to that of a hybrid stepper motor. The rotor is constructed from toothed segments of laminated iron separated by a PM, causing an axial magnetization of the rotor. The magnetic north- and south-pole ends of the rotor are rotationally displaced by a tooth width. The winding layout of the 3-phase (*abc*) motor is presented in figure 2.

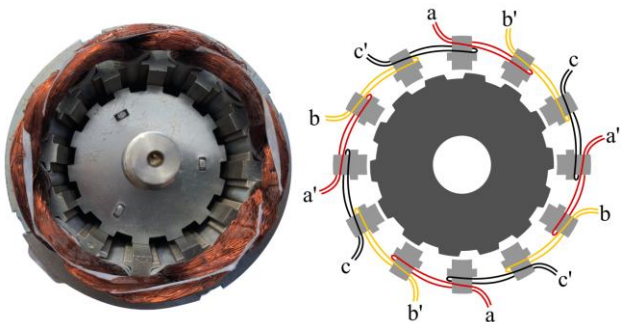


**Fig.2.** Winding layout of the PMSM.

Despite its physical resemblance to the hybrid stepping motor the selected motor may conveniently

be modelled and operated as a conventional PMSM. The theory of operation is outlined in [4].

PMSMs are controlled using a variable frequency drive (VFD), for which the electric circuit is illustrated in figure 3. The VFD uses rectified line voltage to generate the DC bus voltage. The function of the voltage source inverter (VSI) is to distribute the DC bus voltage across the 3 phases of the motor using 6 transistors. These transistors are controlled from a microcontroller ( $\mu C$ ) through pulse width modulation (PWM).

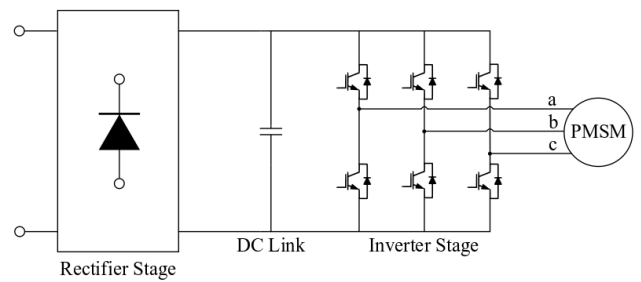


**Fig.3.** Variable frequency drive circuit.

### 3 Dynamic Model of PM Synchronous Motor

For control purposes, a mathematical model of the system is established. An equivalent electrical circuit for the motor is presented in figure 4. The electrical system is modelled as 3 phases connected in a star configuration with a common point between them. Each phase is associated with a resistance ( $R$ ), inductance ( $L$ ) and a back-emf ( $e$ ) component. The back-emf component originates from the coupling of the rotating PMs to the stator windings.

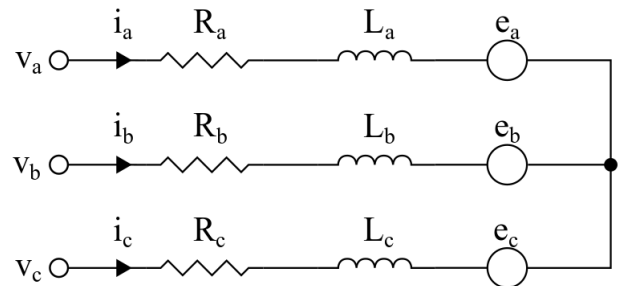


**Fig.4.** Equivalent circuit diagram of the PMSM.

From the equivalent electrical circuit, a coupled set of voltage equations is derived for the system, represented on matrix notation in equation 1.

$$\begin{bmatrix} v_a \\ v_b \\ v_c \end{bmatrix} = \begin{bmatrix} R_a & 0 & 0 \\ 0 & R_b & 0 \\ 0 & 0 & R_c \end{bmatrix} \begin{bmatrix} i_a \\ i_b \\ i_c \end{bmatrix} + \begin{bmatrix} L_a & L_{ab} & L_{ca} \\ L_{ab} & L_b & L_{bc} \\ L_{ca} & L_{bc} & L_c \end{bmatrix} \frac{d}{dt} \begin{bmatrix} i_a \\ i_b \\ i_c \end{bmatrix} + \begin{bmatrix} e_a \\ e_b \\ e_c \end{bmatrix} \quad (1)$$

The voltage equations are coupled due to the mutual inductance between the phases. Introducing an assumption of identical and symmetrically distributed windings, the electrical properties of the phases may be set equal, as shown in equation 2.

$$\begin{aligned} R &= R_a + R_b + R_c \\ L_s &= L_a + L_b + L_c \\ L_m &= L_{ab} + L_{bc} + L_{ca} \end{aligned} \quad (2)$$

Furthermore, due to the star connected configuration of the windings, Kirchhoff's current law (equation 3) may be utilized to decouple the voltage equations.

$$i_a + i_b + i_c = 0 \quad (3)$$

This simplifies equation 1 to equation 4.

$$\begin{bmatrix} v_a \\ v_b \\ v_c \end{bmatrix} = \begin{bmatrix} L_s - L_m & 0 & 0 \\ 0 & L_s - L_m & 0 \\ 0 & 0 & L_s - L_m \end{bmatrix} \frac{d}{dt} \begin{bmatrix} i_a \\ i_b \\ i_c \end{bmatrix} + \begin{bmatrix} R_a & 0 & 0 \\ 0 & R_b & 0 \\ 0 & 0 & R_c \end{bmatrix} \begin{bmatrix} i_a \\ i_b \\ i_c \end{bmatrix} + \begin{bmatrix} e_a \\ e_b \\ e_c \end{bmatrix} \quad (4)$$

A useful property of 3 phase electrical systems are that they may be represented in different reference frames, which is convenient for both modelling and control purposes of such systems. Any 3-phase quantity ( $k$ ) expressed in the  $abc$ -reference can be transformed into an equivalent two-component stationary  $\alpha\beta$ -reference frame. Furthermore, a stationary quantity can be transformed from the  $\alpha\beta$ -reference into a rotating  $dq$ -reference frame. The different reference frames are illustrated in figure 5.

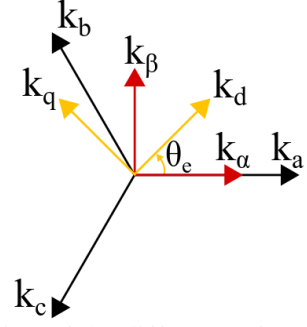


**Fig.5.** Illustration of the different reference frames.

Transformation between the 3-phase  $abc$ -reference and the stationary  $\alpha\beta$ -reference is mathematically realized through the Clarke transformation, shown on matrix notation in equation 5.

$$\begin{bmatrix} k_\alpha \\ k_\beta \end{bmatrix} = \begin{bmatrix} 1 & 0 \\ \frac{1}{\sqrt{3}} & \frac{2}{\sqrt{3}} \end{bmatrix} \begin{bmatrix} k_a \\ k_b \end{bmatrix} \quad (5)$$

Transformation between the  $\alpha\beta$ -reference and the rotating  $dq$ -reference is achieved using the Park transformation, shown in equation 6.

$$\begin{bmatrix} k_d \\ k_q \end{bmatrix} = \begin{bmatrix} \cos\theta_e & \sin\theta_e \\ -\sin\theta_e & \cos\theta_e \end{bmatrix} \begin{bmatrix} k_\alpha \\ k_\beta \end{bmatrix} \quad (6)$$

These transformations can conveniently be applied to the voltage equations, yielding simplified versions of these expressed in the  $dq$ -reference, shown in equation 7. Here  $\omega_e$  denotes the angular velocity of the electrical field,  $\lambda_{PM}$  represents the magnitude of the flux linkage from the PMs and  $L_d$  and  $L_q$  are the  $d$ -axis and  $q$ -axis inductance respectively.

$$\begin{aligned} v_d &= Ri_d + L_d \frac{di_d}{dt} - \omega_e L_d i_q \\ v_q &= Ri_q + L_q \frac{di_q}{dt} + \omega_e L_q i_d + \omega_e \lambda_{PM} \end{aligned} \quad (7)$$

The mechanical system is modelled using Newton's 2<sup>nd</sup> Law. The differential equation describing the dynamics of the mechanical system is presented in equation 8 and relevant quantities are summarized in table 1.

$$J \frac{d\omega_m}{dt} = \tau_e - \tau_L - \tau_{df} \text{sign}(\omega_m) - B\omega_m \quad (8)$$

$\omega_m$	Angular velocity (mechanical)
$J$	Total moment of inertia of the system
$\tau_e$	Developed electro-mechanical torque
$\tau_L$	External load torque
$B$	Coefficient representing the combined losses due to viscous friction and eddy currents
$\tau_{df}$	Torque representing the combined losses due to coulomb friction and hysteresis effects.

**Tab.1.** Symbols

The mechanical and electrical velocity is related through the equivalent number of pole pairs on the rotor ( $p$ ) as shown in equation 9.

$$\omega_e = p\omega_m \quad (9)$$

Based on power considerations, it can be derived that the coupling between the electrical and mechanical systems is as shown in equation 10.

$$\tau_e = \frac{3}{2} p i_q \lambda_{PM} \quad (10)$$

The dynamics of the inverter is assumed to be infinitely fast and therefore negligible. Thus, the previously presented equations are found to provide a complete and sufficient description of the system dynamics. The model parameters have been determined experimentally and are summarized in table 2.

Parameter	Value	
$R$	27.1	[ $\Omega$ ]
$L_d = L_q$	336.7	[mH]
$\lambda_{PM}$	0.35	[Wb]
$J$	0.0796	[kg·m <sup>2</sup> ]
$B$	$3.56 \cdot 10^{-4}$	[Nm·s·rad <sup>-1</sup> ]
$\tau_{df}$	0.019	[Nm]
$p$	14	[-]

**Tab. 2.** Model Parameters.

#### 4 Field Oriented Control

High performance control of PMSM drives is achieved through field oriented control (FOC) techniques. The aim is to regulate the velocity of the system at some predefined reference, while keeping losses at a minimum. The FOC structure is illustrated in figure 6, which shows an inner current-control system cascaded with an outer velocity control loop.

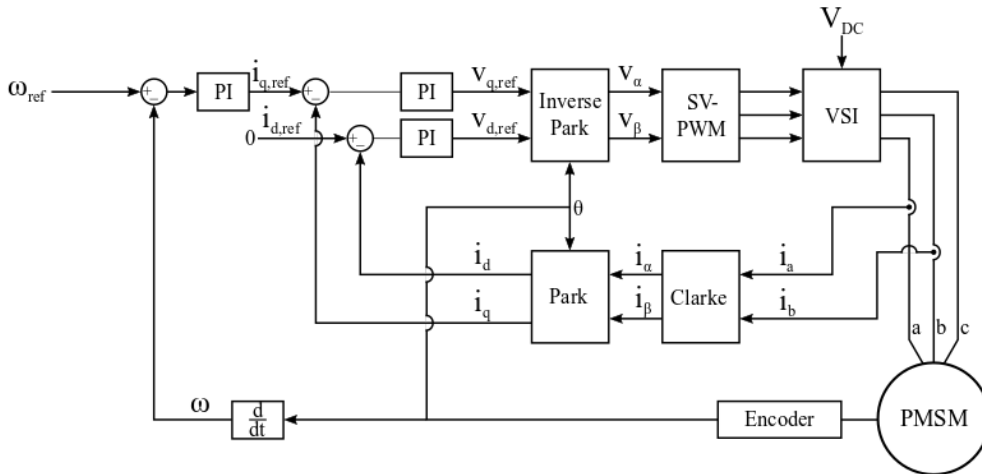


**Fig.6.** Field oriented control structure.

The basic idea of the FOC scheme is to exploit the property that AC quantities in the static reference frame become DC quantities in the rotating reference frame under steady state conditions. Thus, from a control perspective, it is beneficial to have the current control system operating in the rotating  $dq$ -reference. FOC therefore implements the Clarke-Park transformations between the physical 3-phase system and the current control system. From equation 10 it is obvious that only the current component along the  $q$ -axis is generating torque, while the  $d$ -axis current only contributes to the motor losses. Hence, the reference for the  $d$ -axis current is set to 0 and the reference for the  $q$ -axis current is acquired from the velocity controller.

The voltage equations in the  $dq$ -reference were presented in equation 7 and from these the current controllers are designed. Initially it is recognized that these equations are coupled. This coupling is handled using feedforward compensation, as illustrated in figure 7. Consequently, the electrical system may be regarded as being first order and can be controlled with a PI-controller.

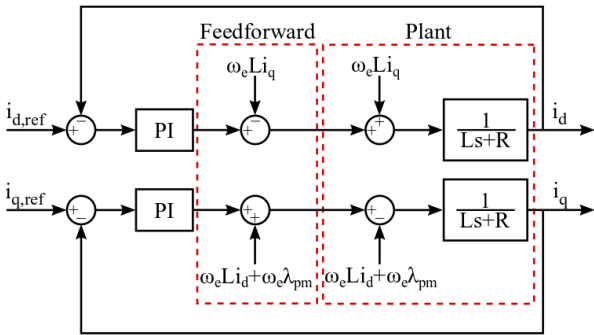


**Fig.7.** Current control loop with feedforward compensation.

The transfer function for the PI-controller is shown in equation 11.

$$G_C(s) = \frac{K_p s + K_i}{s} \quad (11)$$

The design of the current controllers are based on a pole-zero cancellation approach. Hence, the zero of the controller is placed coincident with the pole of the electrical transfer function. Hereafter the controller DC-gain is adjusted to achieve the desired

bandwidth for the system. When using emulation design procedures [5] suggests that if the system is to remain stable upon discretization the bandwidth of the system should be at least 20 times less than the sampling frequency of the feedback signals. It has been found that a sampling frequency of 5 [kHz] is feasible and the current controllers are therefore designed for a bandwidth of 250 [Hz]. This results in current controllers with a proportional gain of  $K_p=530$  and an integral gain of  $K_i=4.2 \cdot 10^4$ .

When doing cascade control it is essential to have the inner loop significantly faster than the outer loop. [5] suggests that the inner loop should be at least 10 times faster, so that the dynamics of the inner loop can be neglected when designing the controller for the outer loop. Assuming this condition to be satisfied, the velocity loop can be regarded as shown in figure 8. The transfer function for the mechanical system is derived from equations 8 and 10, while the load torque ( $\tau_L$ ) and the static torque ( $\tau_{df}$ ) are considered disturbances.

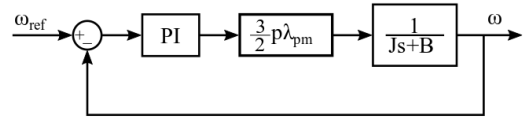


**Fig.8.** Outer velocity control loop.

It is noted that the mechanical system, like the electrical system, is modelled as being first order and therefore similar design procedures are used for designing the PI-controller for the outer loop. The controller zero is thus placed coincident with pole of the transfer function for the mechanical system and then the DC gain is adjusted so that the bandwidth for the outer loop is 10 times slower than the inner loop, equivalent to 25 [Hz]. This results in velocity controllers with a proportional gain of  $K_p=0.56$  and an integral gain of  $K_i=25 \cdot 10^4$ .

The closed loop step responses for both the current and velocity loops are shown in figure 9. The response of the current loop is characterized by a rise time of 0.001 [s] and no overshoot. The response of the velocity loop is characterized by a rise time of 0.04 [s] and no overshoot. No overshoot in the response of the system is favorable as to protect the electrical and mechanical components

from excessive wear. The overall dynamic performance of the control system is found acceptable and appropriate for implementation in the physical system.

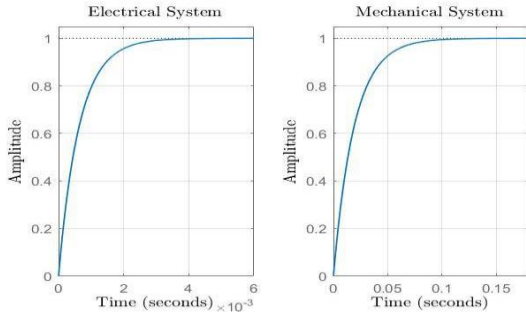


**Fig.9.** Closed loop step response.

The current controllers output voltage references in the  $dq$ -reference. These references are first transformed into equivalent  $\alpha\beta$ -voltage references, using the inverse Park-transformation, and subsequently converted into physical 3-phase signals using a space vector modulation (SV-PWM). SV-PWM allows the direct transformation of a voltage reference vector in the stationary  $\alpha\beta$ -frame into appropriate PWM signals that can be transmitted from the DSP to the 6 transistors on the VSI. The basic principle of SV-PWM is that there are eight feasible transistor configurations (base vectors) for the 3-phase VSI. These include six non-zero vectors that can be projected onto the  $\alpha\beta$ -frame and two zero vectors. The base vectors and their corresponding transistor configurations are illustrated in figure 10, where green represents a transistor in the ON state and grey represents a transistor in the OFF state. Any generated reference vector ( $v_{\alpha\beta}$ ) will thus be positioned in one of six possible sectors in the  $\alpha\beta$ -frame. The SV-PWM algorithm then seeks to decompose this reference vector into duty cycles ( $d$ ) for the neighboring base vectors, based on the angle ( $\varphi$ ) and magnitude ( $|v_{\alpha\beta}|$ ) of the reference vector. This is exemplified in figure 9 with a reference vector placed in sector 1. This is then decomposed into duty cycles ( $d$ ) for base vectors  $V1$  and  $V2$ . This means that over a predefined time period ( $T$ ) the reference vector can be generated by applying  $V1$  for a time of  $d1 \cdot T$  and  $V2$  for a time of  $d2 \cdot T$ , while the remaining time is spent on one of the zero vectors. The two zero vectors are used alternately, as a means of distributing the wear on the transistors.

The actual mathematical implementation of the SV-PWM algorithm is based on the min-max method as presented in [6], which is suggested to require less processor power in the DSP.

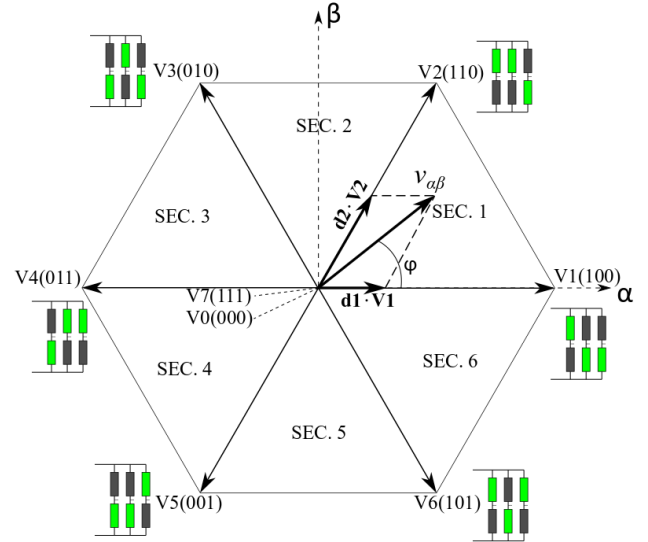


**Fig.10.** Space Vector Modulation.

## 5 Control System Implementation

A schematic diagram showing the implementation of the control system is presented in figure 11. Besides the PMSM, the implementation is based on three central pieces of hardware, besides the previously presented PMSM. These include a 2 [kW] inverter board based on the Infineon IRAM630-1562F 15 [A], 600 [V] IGBT power module and with integrated Honeywell CSLW6B1 current sensors. Additionally a SCANCON 2RK rotary encoder with a resolution of 2000 [pulses/rev] is used for position and velocity feedback measurements. Finally a STMicroelectronics STM32F103C8 microcontroller with dedicated motor control peripherals is selected for the digital implementation of the control system. The peripherals include a PWM module as well as an encoder module, which are of obvious relevance. Due to resource constraints, the rectifier circuit is not included as part of the implementation and the DC link is therefore generated by a laboratory DC power supply.

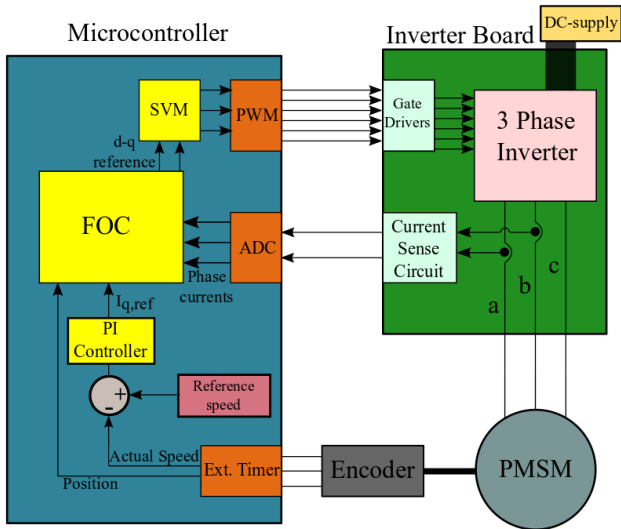


**Fig.11.** Schematic diagram of the control system implementation.

A detailed description of the digital implementation on the microcontroller and how the software is structured is presented in [4]. Key features of implementing the control system digitally involves discretization of the controllers, setting up the PWM module and acquiring the feedback signals. The controllers are discretized using the bilinear transform, which approximates a discrete controller transfer function ( $G(z)$ ) from a continuous controller transfer function ( $G(s)$ ) through the relation shown in equation 12.

$$G(z) = G(s) \Big|_s = \frac{2}{T_s} \left( \frac{z-1}{z+1} \right) \quad (12)$$

Here  $T_s$  is the sampling time for the digital control system, specified to 0.2 [ms].

The PWM module is configured to operate with a triangular carrier wave, as shown in figure 12. The carrier wave is generated by setting up a timer to perform an up-down count. The carrier wave is configured to a frequency of 5 [kHz], resulting in a switching frequency for the transistors of 10 [kHz], which is below the maximum recommended switching frequency of 20 [kHz] for the transistors. The compare value is generated based on the duty cycles computed by the SV-PWM algorithm. The carrier wave is additionally used to generate an interrupt for the current measurement. The interrupt

is configured to occur when the carrier wave reaches its maximum due to two reasons. These are that the current at this point in the PWM cycle will be at an average value and also the disturbance from the transistor switching is minimized, as illustrated in figure 8. The current is measured by configuring the microcontroller's 12bit ADC.

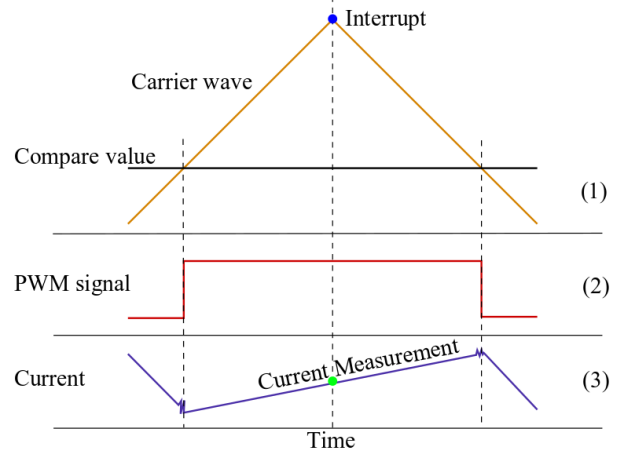


**Fig.12.** PWM generation and current measurement.

The position and velocity feedback measurements are realized by setting up an external timer to count the encoder ticks from the two channels on the encoder. The position is computed directly from the tick count and configured to operate within a working interval of 0 to  $2\pi$ . The velocity is computed by measuring the number of encoder ticks over a predefined sampling time. To obtain a satisfactory accuracy on the velocity measurements it is found sufficient to measure the velocity feedback signal with a sampling frequency of 166 [Hz].

Final implementation considerations involve PWM dead time and velocity reference generation. To protect the DC link from being shorted, it is essential that the two transistors on the same inverter leg are not conducting simultaneously. Since the transistors do not have infinitely fast transients, it is necessary to introduce dead time between the PWM pulses. Dead time ensures that the conducting transistor has sufficient time to turn off before the opposite transistor switches on. The dead time is determined according to the dynamic response of the transistors, i.e. how fast the transistors turn on and off. Lastly, the velocity reference is considered. Stepping the

velocity reference will result in large peak currents and large accelerations. This will cause significant strain on both the electrical hardware as well as the mechanical components, which is found undesirable. Instead the velocity reference is ramped up and down, to protect the system components from unnecessary wear.

## 6 Model Validation

Having implemented the control system digitally the simulation model can be validated experimentally. The approach for validating the model is to compare the predicted closed loop step response of the simulation model with the actual response of the physical system, when both are implemented with identical controllers. The pulse width modulation has not been included in the simulation model, and the simulated response therefore doesn't include modulation effects. Furthermore, the simulation model does not include measurement noise and inverter dynamics. These limitations of the model are expected to show during validation and should be considered when comparing the model response to the physical system. The controllers used for model validation are downscaled version of the previously designed controllers, which yield a slower dynamic response. This is found necessary as to ensure a sufficient number of samples during the rise time, and thus an improved basis for comparison.

First part of the validation deals with the electrical system, i.e. the inner current control loop. The electrical system is validated by stepping the  $d$ -axis current reference and comparing the model and physical closed loop response, when both are implemented with identical controllers. Comparison of the actual and simulated response to a step input in the  $d$ -axis current shows good correlation between the model and the actual system, as shown in figure 13. The model of the electrical system is found to provide a satisfactory description of the actual system dynamics and it is therefore not found necessary to modify the electrical model parameters.

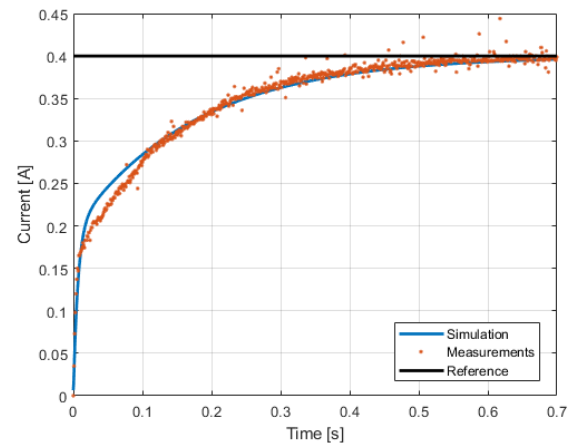


**Fig.13.** Comparison of simulated and measured  $d$ -axis current step response.

Having validated the inner current control loop, next the mechanical system is subjected to validation procedures. This is similarly done through comparison of the actual and simulated closed loop responses, with implementation of identical controllers. Comparison between the physical and the model response to a step input in the velocity reference is shown in figure 10. The simulated and actual response generally shows good correlation, however some deviation between the responses do exist. This deviation is assessed to be the combined effect of uncertainties in the model parameters, non-linearities in the physical system that have not been modelled and measurement noise in the physical. Yet, the deviations between the model and the physical system are not deemed large enough to justify an alteration of the mechanical model parameters.

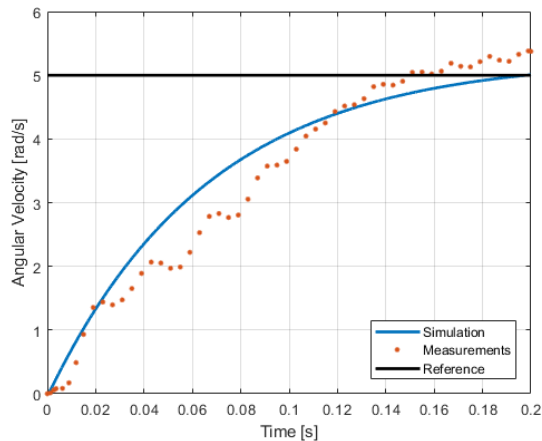


**Fig.14.** Comparison of simulated and measured velocity step response.

## 7 Application Evaluation

Having designed and implemented the PMSM drive the framework for evaluating the relevance of the PMSM drive for the cow brush application has been established.

The PMSM drive is benchmarked against a typical geared IM commonly found in commercial cow brush devices. The specific IM motor used for benchmarking is a line fed 230 [V], 370[W], 1400 [rpm] 4-pole single-phase permanently split capacitor type IM combined with a 40:1 worm gearing. Two performance tests are set up to investigate the comparative performance between the designed PMSM drive system and the specified IM system. These tests involve an experimental investigation of the power consumption at no-load and the efficiency of the brush at a predefined load level.

The power consumption at no-load provides an indication of how much energy is required simply to keep the brush rotating at steady state. This is experimentally investigated by running the brush without load at an output speed of 35 [rpm] under steady state conditions, while recording the consumed electrical power using a PM100 single-phase power analyzer. The results of the no-load power consumption test showed that the IM-based transmission system consumes approximately 300 [W], while the PMSM-based transmission system only consumes 9 [W].

It is found that a realistic load level for the cow brush is characterized by a load torque of up to 25 [Nm] acting on the brush shaft. Using this load reference combined with a steady state output speed of 35 [rpm] the efficiency of the device is investigated. For the IM-based transmission system a force transducer is implemented in the system from which the torque can be measured directly, while the velocity is measured using an encoder. The product of these yield the system output power, which is divided with the electrical input power measured using the power analyzer. The efficiency of the IM system at these prescribed conditions is measured to be approximately 21 [%].

During implementation of the designed PMSM drive system significant issues were encountered related to noise on the measured feedback signals. These issues are documented and discussed in [4]. The noise related issues were of particular significance to the performance of the control system when attempting to load the brush heavily. Consequently, it has not been possible to investigate the efficiency at the prescribed load level of 25 [Nm] on the physical PMSM system. Instead the efficiency is approximated using the validated simulation model of the system. It is recognized that this procedure is associated with large uncertainties and the result may not provide an accurate measure of the efficiency for the actual PMSM system. Therefore conservative estimates of the losses not captured by the model are additionally included in the estimate for the PMSM system efficiency. This yields a conservative efficiency estimate for the PMSM system of 73 [%].

## 8 Conclusion

The objective of this paper has been to investigate the potential of introducing a PMSM drive system in a cow brush to reduce the energy consumption of the device. For this an experimental setup has been constructed by implementing PMSM drive system in a commercial cow brush. For this setup a control system has been designed and implemented digitally.

Evaluation of the designed PMSM system is done through comparison against an IM system typically used for commercial cow brush applications. The no-load power for the IM system was found to be 300 [W] compared to only 9 [W] for the PMSM system. Additionally the efficiency of the IM system was measured at only 21 [%] compared to an estimated 73 [%] for the PMSM system.

Based on these results this paper concludes that there are evident rewards in driving the system with a PMSM-based transmission system rather than the commonly favored IM-based transmission system with respect to energy savings. The PMSM system provides both a remarkably higher efficiency upon loading and a significantly lower no-load power consumption. However there are still a number of issues that need to be considered regarding the test setup for the PMSM system to become an actual feasible solution for final implementation in a cow brush. Furthermore, the IM system provides a more rugged transmission system solution and it is expected to have lower initial cost as compared to the PMSM system. These factors are not addressed in this paper, however should be considered before making a potential transition from the IM system to the PMSM system.

### Acknowledgement

The authors of this work gratefully acknowledge Grundfos for sponsoring the 6<sup>th</sup> MechMan symposium. The authors would also like to direct a sincere thanks to GEA Farming Technologies Mullerup for the project collaboration.

### References

- [1] R. Brown "Benefits and Pitfalls When Using Permanent Magnet Motors in Spinning Applications". *IEEE*, 2002.
- [2] "Technical Advantages of a Permanent Magnet Brushless System". MOOG – Aspen Motion Technology. Web, 2018.
- [3] E. Metzger "Making the case for cow brushes". Progressive Dairyman, 2015.
- [4] S. Borup, M. Brandt, F. Clausen, A. Langbak, A. Torp "Concept Study of PM Synchronous Motor in Cow Brush Application". Semester Project Report. Aalborg University, 2018.
- [5] C. Phillips and J. Parr "Feedback Control Systems". Prentice Hall, 2011.
- [6] V. Blasko "Analysis of a Hybrid PWM Based on Modified Space-Vector and Triangle-Comparison Methods". *IEEE Transactions on Industry Applications*, Vol. 3, pp 756-764, 1997.